Integrated Microwave Photonics Coherent Processor for Massive-MIMO Systems in Wireless Communications

Pablo Martínez-Carrasco Romero ⓘ, José Roberto Rausell-Campo ⓘ, Diego Pérez-Galacho ⓘ, Xu Li ⓘ, Ting Qing, Tiangxiang Wang, and Daniel Pérez-López ⓘ, *Member, IEEE*

Abstract—**Massive-MIMO systems can achieve high capacities and data rates by increasing the number of operational antennas in the base station. As more antenna elements are introduced, the complexity of the signal processing operations increases accordingly and current electronic processors struggle to reach those requirements. To overcome these hurdles, we propose a novel theory to process the RF signals in the optical domain. We experimentally demonstrate the capabilities of theory using a non-integrated Dual Parallel Modulator as a 2×2 optical matrix multiplier, recovering satisfactorily previously mixed RF signals modulated following the standards in 5G communications. Finally, we propose an integrated photonic architecture based on a core of Mach Zehnder Interferometers to physically process the information. Together with the optical core, we proposed the integration of RF modulators, microwave photonic filters and high-speed photodetectors. We present simulations on the expected performance of the circuit and analyze the impact of fabrication errors.**

Index Terms—**Coherent photonic processor, integrated microwave photonics, Mach Zehnder interferometers, massive-MIMO, photonic MIMO, wireless communications.**

I. INTRODUCTION

IT IS undeniable that large scale wireless telecommunications are playing a great role in our day to day. Together with the current deployment of the 5G network, we will face an increasing demand for high capacity, high data rates and low latencies coming from the introduction of emerging Internet of

Pablo Martínez-Carrasco Romero, José Roberto Rausell-Campo, Diego Pérez-Galacho, and Daniel Pérez-López are with the Photonics Research Labs, Universitat Politècnica de València, 46022 Valencia, Spain, and also with the Institute of Telecommunications and Multimedia Applications, Universitat Politècnica de València, 46022 Valencia, Spain (e-mail: pmarrom@iteam.upv.es; joraucam@upv.es; diepega@upv.es; daniel.perez@ipronics.com).

Xu Li, Ting Qing, and Tiangxiang Wang are with the Ottawa Wireless Advanced System Competency Centre, Huawei Technologies Canada Co., Ltd., Ottawa, ON K2K 3J1, Canada (e-mail: lixu11@huawei.com; qingting1@huawei.com; wangtianxiang@huawei.com).

Things (IoT) services, autonomous vehicles, artificial intelligence, smart cities and the development of the future 6G [1], [2]. An improvement in the capabilities of current available technologies and the development of novel systems will be essential to reach the required specifications [3]. One of these technologies is the Multiple-In Multiple-Out (MIMO) that has been one of the enablers of the evolution of the past LTE and is being adapted to bring in large-scale antenna arrays with hundreds or thousands of antennas in order to optimize the operation with mmWave carrier frequencies [4], [5].

Massive-MIMO systems allow the transmission of several signals over the same radio channel augmenting the capabilities of the system and achieving high spectral efficiencies and low latencies. To fully harness these benefits, high dimensional processing operations are required [6]. This requires not only a great computational capacity but also large power consumption [7], [8]. Current approaches rely on Digital Signal Processors (DSP), but electronic processors present some intrinsic limits in terms of bandwidth and efficiency [9], which, together with the end of the Moore's era [10] makes necessary the exploration of alternative ways of computation. A possible solution may be found in photonics. Photonic systems are immune to electromagnetic interference and have some advantages over electronic devices such as high bandwidths, high parallelism and low latency. The processing of RF signals in the optical domain have been deeply studied and promising results can be found in the literature. High-speed modulators, RF filters, delay lines and beamforming networks have been experimentally demonstrated [11]. Moreover, general purpose microwave photonic processors that can be reconfigured via software have also been proposed [12], [13].

For the case of MIMO processing the main purpose is to unscramble the received RF signals that have been mixed due to interference during their free space propagation. There have been multiple attempts to solve this problem aided by photonic systems. Interference cancellation, where the signal of interest is separated from added noise have been experimentally demonstrated using tunable delays [14], [15], semiconductor optical amplifiers [16], [17], dispersive elements [18], microring resonators (MRRs) [19] or the nonlinear response of optical modulators [20]. Furthermore, a more general scheme based on the broadcast-and-weight (B&W) protocol using MRRs to perform the matrix multiplications in optical domain have been

theoretically studied and great improvements in terms of bandwidth and energy consumption over DSP systems have been calculated [21].

In the following work we present a coherent architecture based on meshes of integrated Mach Zehnder Interferometers (MZIs) on a Silicon-on-Insulator platform instead of microring resonators to perform matrix multiplications in parallel. One of the advantages of interferometric approaches over the B&W protocol is that complex transformations can be directly implemented without any pre- or post- processing. MZI meshes can perform any unitary transformation $|y\rangle = U|x\rangle$ and can be extended to any general linear transformation via Single Value Decomposition (SVD) [22]. This type of linear architectures has been previously implemented for deep learning [23], quantum computing [24] or Ising machines [25]. Mode scrambling due to crosstalk in multimode fibers has been also tackled with these systems [26], [27], [28]. We will extend the photonic matrix multiplier core by adding high-speed RF modulators, photonic filters and high-speed photodetectors to adapt the system to the requirements of massive-MIMO systems.

This work brings as a novelty the combination of previous investigated ideas, that is, photonic matrix multiplication, up-down conversion of RF signals and photonic assisted RF signal processing, in the context of wireless MIMO communications. More concretely, two key concepts have been added to the standard optical matrix multipliers. First, the introduction of microwave photonic filters for the suppression of the optical carrier and one of the RF sidebands. Second, the reinjection of the optical carrier for the recovery of the amplitude and phase with direct photodetection. To the best of our knowledge, there is no work that demonstrates both theoretically and experimentally the benefits of photonics-based RF MIMO and analyse the limitations and necessary upgrades of the integrated components to achieve a full competitive position.

The remaining of this article continues as follows. In Section II, we introduce the basics of the RF MIMO. In Section III, we develop the theory of up-converting the RF signal into the optical domain and unscrambling the corresponding signals with a coherent analog processor and direct photodetection. We study the need for side-band and carrier filtering to maintain the phase information of the RF signals. In Section IV, we carry out an experimental demonstration of the presented theory in a non-integrated optical setup. Finally, in Section V we show the proposed architecture and explained the different modules, along with theoretical simulations of the performance of the architecture.

II. MIMO RF THEORY

Consider a massive-MIMO uplink system with t single-antenna transmitters and a Base Station (BS) equipped with r receiving antennas, where the channels between the users and the BS are modelled as narrowband time-invariant wireless channels with Rayleigh fading. The behaviour of the channel is described by the deterministic matrix [29], [30] $H \in \mathbb{C}^{r \times t}$.

The theoretical development has been made using Dirac's notation which simplifies expressions and calculations when
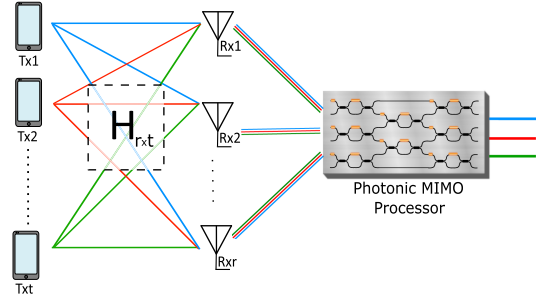
Fig. 1. Schematic of the complete system. Several RF signals are sent through a physical channel. In the process of propagation, the signals are mixed thus each antenna on the reception receives a linear combination of the original signals. The output of these antennas is up-converted to the optical domain on the photonic MIMO processor (more details in Fig. 9), where the changes of the channel on the RF signals are undone. Finally, the original wireless signals are recovered.

working with vectors and matrices. If we take a sample of a discrete time instant we can express the received signal at the BS as follows:

$$|Y\rangle = H|X\rangle + |n\rangle \quad (1)$$

Where $|X\rangle \in \mathbb{C}^{t \times 1}$ denotes the transmitted signal, with any modulation, $|Y\rangle \in \mathbb{C}^{r \times 1}$ denotes the received signal and $|n\rangle \in \mathbb{C}^{r \times 1}$ represents the white symmetric Gaussian noise, $|n\rangle \sim N(0, \sigma^2)$. After the signals transmitted by the users are received, the objective is to obtain the best estimation of the signal transmitted by each user, $|\hat{X}\rangle$, by solving the following optimization problem:

$$|\hat{X}\rangle = argmin_X ||Y\rangle - H|X\rangle| \quad (2)$$

Different detection schemes have been proposed in the literature e.g. linear methods as Zero Forcing (ZF) or Minimum Mean-Square Error (MMSE). These methods follow the same idea, multiply by a matrix A that cancels the interaction with the channel to the greatest extent.

$$|\hat{X}\rangle = A|Y\rangle = AH|X\rangle + A|n\rangle \quad (3)$$

Traditionally, MIMO models in wireless communications have been performed in the digital domain since there is no way to linearize the received signal in the analog domain it becomes impossible to perform the required matrix multiplications. Photonics brings us the possibility of performing this matrix multiplication analogically in the optical domain, taking advantage of the fact that an interaction between electromagnetic fields occurring in RF can be undone optically, see Fig. 1.

III. PHOTONIC SIGNAL PROCESSING

We start from the RF matrix signal received at the BS, $|Y\rangle$. The original signal $|X\rangle$ was modeled as an analytical signal, which has undergone changes in the channel in the form of attenuations, combinations and phase shifts, so the received signal is also analytical. Using optical amplitude modulators the RF signal is up-converted into the optical domain. For the development of the theory we assume a perfectly linear double-sideband modulation of the optical field. Although this approach may seem unrealistic,

the field of linearization and filtering of modulated signals has been extensively studied and has very advanced linearization techniques if needed [31]. At first stages of study this approximation gives satisfactorily accurate results (see Section IV). Optical modulation can be expressed mathematically as follows:

$$|S\rangle = e^{i\omega_0 t} \left[\begin{bmatrix} 1 \\ 1 \\ \vdots \\ 1 \end{bmatrix}_{r \times 1} + m\Re\left[|Y\rangle\right] \right] = e^{i\omega_0 t} \left[|\alpha\rangle + m\Re\left[|Y\rangle\right]\right]$$

$$(4)$$

Where the exponential term represents the optical laser multiplying a vector formed by ones and the vector formed by the received analytical signal together with the modulation index m. The unit vector is just a mathematical tool used for the representation of the optical carrier in an specific time instant. We will denote it as $|\alpha\rangle \in \mathbb{N}^{r,t \times 1}$ and its dimension depends on the dimension of the vector to which it is added. The symbol $\Re$ denotes the real part of the element.

At this point we must operate on the modulated signals, applying the appropriate combinations and phase shifts in a matrix manner to undo the changes produced by the channel. However, if a modulated signal passes through an optical phase shifter, it acquires a phase shift which will be lost on the photodiode due to the square-law of the photodetection process, assuming an envelope detector. Because of that, in order to see changes on the RF signal by applying changes on the optical signal we must filter out the optical carrier and one of its side-bands, allowing for just single-side band (SSB) with carrier suppression propagation through the optical computational tool. After this operation the optical carrier must be re-inserted with the objective of generate a photocurrent with a phase shift in the microwave domain equal to the phase shift in the optical domain [32]. In order to maintain the phase coherence of the complete signal both filtering and carrier re-injection must be done on-chip. A possible option could be splitting the optical carrier on-chip before modulation, so the re-injection preserves the phase of the signal.

Mathematically, filtering carrier and side-band is equivalent to eliminating $|\alpha\rangle$ and recovering $|Y\rangle$ as an analytical signal with half the intensity, since one of the side-bands has been lost.

$$|S_F\rangle = e^{i\omega_0 t} \left[\frac{m|Y\rangle}{2} \right] \qquad (5)$$

After the filtering stage we can operate with the mathematical tool that performs matrix multiplication.

$$|\hat{S_F}\rangle = e^{i\omega_0 t} \left[\frac{m}{2} A|Y\rangle \right] = e^{i\omega_0 t} \left[\frac{m}{2} |\hat{X}\rangle \right] \qquad (6)$$

On the resulting side-band there is the information of the estimated transmitted signal. We can recover these RF signals after re-injecting the optical carrier and performing direct photodetection.

$$|\hat{S}\rangle = e^{i\omega_0 t} \left[\begin{bmatrix} 1 \\ 1 \\ \vdots \\ 1 \end{bmatrix}_{t \times 1} + \frac{m}{2}|\hat{X}\rangle \right] = e^{i\omega_0 t} \left[|\alpha\rangle + \frac{m}{2}|\hat{X}\rangle\right] \quad (7)$$

Envelope photodetection can not be expressed as a matrix, it must be calculated element by element. As a general result, the photodetected current of the signal in an instant t at the output k would be:

$$I_k = |\hat{S}_k|^2 = e^{i\omega_0 t} \left[\alpha_k + \frac{m}{2}\hat{X}_k\right] e^{-i\omega_0 t} \left[\alpha_k + \frac{m}{2}\hat{X}_k^*\right]$$

$$= 1 + \frac{m^2}{4}|\hat{X}_k|^2 + m\Re\left[\hat{X}_k\right] \qquad (8)$$

Discarding the direct current term and filtering the high order RF frequencies, that result from the signal-to-signal beat noise, we can recover the transmitted information from $\Re[\hat{X}_k]$.

A. Alternative Cases: Filtering Just one SB

Carrier filtering and reinsertion is performed to avoid unwanted rotations of the signals at the different outputs of the matrix. Usually, in classical wireless communications there is the presence of Phase Locked Loops (PLLs), responsible for coordinating the arrival phase of the incoming signal and correctly orienting the received constellation. On the ideal case of having a PLL on the output of each photodetector it would not be necessary filtering and reinserting the carrier, it would only be necessary to use SSB modulation before photodectection, resulting on an easier design in the photonic processor.

$$|S_F\rangle = e^{i\omega_0 t} \left[|\alpha\rangle + m|Y\rangle\right] \qquad (9)$$

By filtering only one of the sidebands we recover the received analytical signal with half the intensity and still keeping the contribution from the optical carrier. Then, just as in the previous case, we operate the mathematical tool to estimate the original sent signal.

$$|\hat{S}\rangle = e^{i\omega_0 t} \left[A|\alpha\rangle + \frac{m}{2}A|Y\rangle\right] = e^{i\omega_0 t} \left[A|\alpha\rangle + \frac{m}{2}|\hat{X}\rangle\right]$$

$$(10)$$

$$\hat{S}_k = e^{i\omega_0 t} \left[\sum_{j=1}^{r} A_{kj}\alpha_j + \frac{m}{2}\hat{X}_k\right] \qquad (11)$$

$$I_k = \left|\sum_{j=1}^{r} A_{kj}\right|^2 + \frac{m^2}{4}|\hat{X}_k|^2 + m\Re\left[\sum_{j=1}^{r} A_{kj}\hat{X}_k\right] \quad (12)$$

In this case the multiplication $A|\alpha\rangle$ alters the value of the DC term after photodetection, as well as the amplitude and
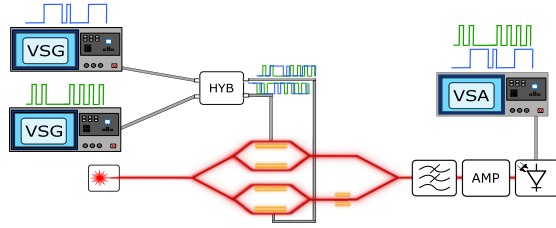
Fig. 2. Experiment scheme. Using two Vector Signal Generators we generate the independent RF signals which will be combined using the different hybrids. Both mixed signals are up-converted on the Dual-Parallel and with the phase shifter from one of its arms we can undo the combination caused by the hybrids.

Fig. 3. Spectrum 90° for a phase shift between the arms of the DPMZM of (a) $-\pi/2$, (b) 0, (c) $\pi/2$ and (d) π degrees. We can recover both tones with a power difference of 30 dB.

phase of the photodetected signals. This effect would worsen the information of the received signals, mainly due to the presence of noise.

IV. PROOF OF CONCEPT: EXPERIMENTAL DEMONSTRATION

As a proof of concept, we experimentally demonstrate the theoretical proposal in Section III. We implemented known RF channels in order to undo its changes in optical domain. Two hybrid couplers, $90°$ and $180°$, have been used to simulate the channels. Although these are very low-dimensional and simple matrices, they serve to demonstrate the possibility of operating in the optical domain to undo the changes of RF signals.

In both cases we implement 2×2 matrices, which combine the signal produced by two different signals, with the possibility of using different frequencies, bandwidths and modulation schemes.

Assuming a channel without noise and known by both the receiver and the transmitter, the implementation of the estimation matrix is very simple, especially considering that these are square matrices. Therefore, for the particular case of our experimental set-up $A = H^{-1}$.

The RF signals were generated using two different Vector Signal Generators (VSGs), E8267 C PSG Agilent and SMW200 A Rhode & Schwarz. Both signals are mixed usign the hybrids and each one of the outputs is up-converted to the optical domain. For this up-conversion we used a Dual-Parallel Single-Drive Mach-Zehnder modulator (DPMZM) where each one of the IQ modulators is driven simultaneously and independently with the RF signals from the outputs of the hybrids. Notice that this is not the common use for a DPMZM, we are feeding each arm with different RF signals. The idea is to use the DPMZM as two independent Single-Drive Mach-Zehnder modulators biased in quadrature and implement at the same time the desired matrix multiplication by tuning the bias voltage. After this operation, the resulting optical signal gets transformed back to the RF domain using a photodetector. Finally, we use a Vector Signal Analyzer (VSA), SMW200 A Rhode & Schwarz, to study the resulting signal.

Since we just can study the outputs separately and our VSA has a PLL implemented we only need to perform the single side band filtering described in Section III-A. An scheme of the experimental set up is shown in Fig. 2.
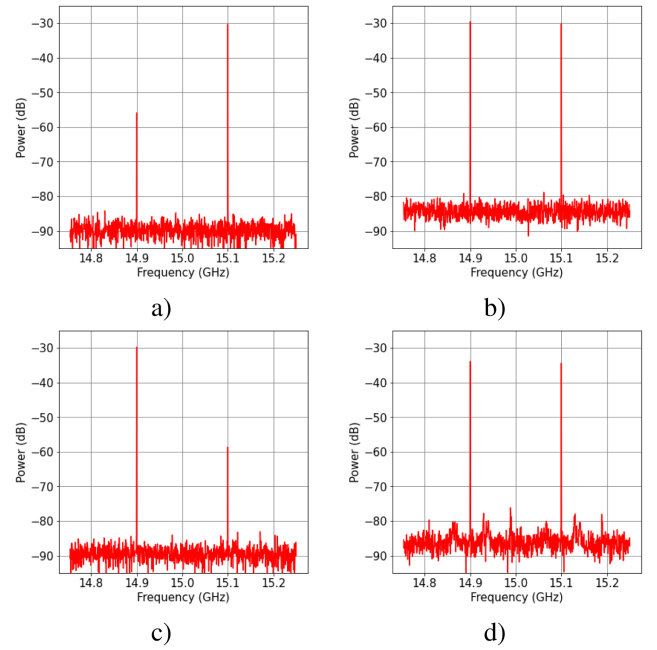
A. Hybrid $90°$

The Hybrid coupler $90°$ can be expressed as a matrix in terms of electromagnetic fields as follows:

$$H = \frac{1}{\sqrt{2}} \begin{bmatrix} 1 & i \\ i & 1 \end{bmatrix} \tag{13}$$

In order to implement the inverse matrix with the DPMZM we set one arm with a phase shift of $\pm\pi/2$ with respect to the other and we sum both signals.

$$A|\alpha\rangle = H^{-1}|\alpha\rangle = \frac{1}{\sqrt{2}} \begin{bmatrix} 1 & -i \\ -i & 1 \end{bmatrix} \begin{bmatrix} 1 \\ 1 \end{bmatrix} = \frac{e^{-i\frac{\pi}{4}}}{\sqrt{2}} \begin{bmatrix} 1 \\ 1 \end{bmatrix} \tag{14}$$

$$\sum_{j=1}^{2} A_{kj}\hat{X}_k = \frac{1}{\sqrt{2}}(1-i)\hat{X}_k = \frac{e^{-i\frac{\pi}{4}}}{\sqrt{2}}\hat{X}_k \tag{15}$$

As shown in (14) and (15), after the photodetector both signals presents the same DC term and undergo the same phase shift resulting in a rotation of the received constellation, which is easily correctable by our Vector Signal Detector with the PPL. To check that our scheme worked, we started by sending two RF tones at different frequencies looking for separate them at the output of the modulator. We found that by adding the predicted phase shift between arms we could recover both RF tones independently achieving a suppression of 30 dB of one of the tones with respect to the other as shown in Fig. 3. This suppression corresponds to the extinction ratio of the DPMZM.
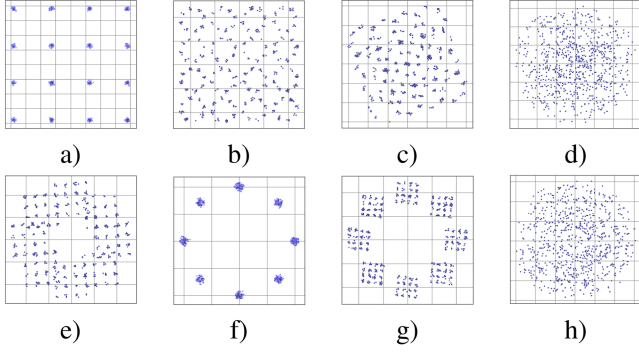
Fig. 4. Constellation evolution using 90° hybrid. We can see how the signal changes depending on the phase applied by the modulator[(a) to (h)], going from (a), a perfect 16QPSK in −π/2, to (f) an 8PSK in π/2. Both constellations disappear completely when we are in the phases that combine both signs equally, 0 and π in (d) and (j).
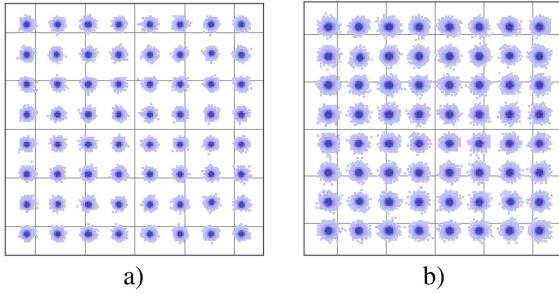
Fig. 5. Constellation for 5G signals at 50 MHz (a) and 100 MHz (b) for 90° hybrid.

After this first test we tried a more complex experiment related directly with MIMO technology. We modulate two different RF signals with the same frequency, 15 GHz, and bandwidth, 20 MHz. Seeking to discern between both signals, we modulate them following 16QPSK and 8PSK modulation, the evolution of both constellations is shown in Fig. 4.

As seen in the spectrum of Fig. 3, when the phase shift added by the dual-parallel modulator is ±π/2 we can separate perfectly the original modulated signals. Following the same procedure, we recover the constellation of the two signals. The evolution of the received signals as a function of the applied phase is depicted in Fig. 4 where the noisy mix of both signals can be seen when we apply a phase different from ±π/2. The same measurements can be performed on 5G signals, in this case for 50 and 100 MHz bandwidths. The constellations of the signals after their separation is shown in Fig. 5. This reaffirms the possibility of using optical processing to drive MIMO processing in the next generations of wireless communications.

B. Hybrid 180°

Similar to the 90° hybrid, with the 180° hybrid we can separate the original signals using the optical modulator, just adding or subtracting the optical signals. In other words, adding a relative
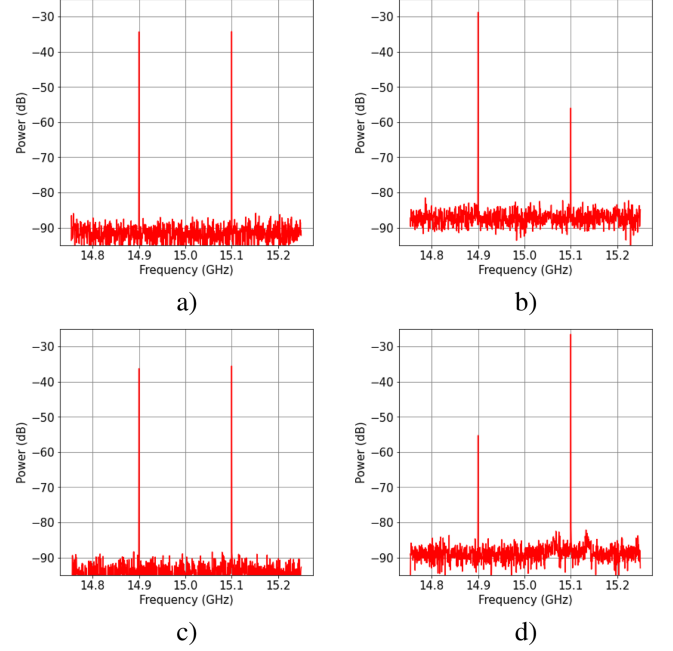
Fig. 6. Spectrum 180° for a phase shift between the arms of the DPMZM of (a) −π/2, (b) 0, (c) π/2 and (d) 0 degrees after changing the input ports. We can recover both tones separately at the sum output of the estimation matrix.

phase shift between arms of 0 or π degrees.

$$H = \frac{1}{\sqrt{2}} \begin{bmatrix} 1 & 1 \\ -1 & 1 \end{bmatrix} \quad (16)$$

In this specific case, when multiplying by the estimated matrix one of the output signals disappears because the carrier is canceled when the modulated signals are added in counter phase, despite of the imperfections on the hybrid and the actuation of the amplifier we are not able to recover this signal. As a result of this we changed the input ports of the RF signals to the modulator, seeing that way only the sum output of the estimation matrix.

$$A|\alpha\rangle = H^{-1}|\alpha\rangle = \frac{1}{\sqrt{2}} \begin{bmatrix} 1 & -1 \\ 1 & 1 \end{bmatrix} \begin{bmatrix} 1 \\ 1 \end{bmatrix} = \frac{1}{\sqrt{2}} \begin{bmatrix} 0 \\ 2 \end{bmatrix} \quad (17)$$

$$\sum_{j=1}^{2} A_{1j} \hat{X}_1 = \frac{1}{\sqrt{2}} (1 - 1) \hat{X}_1 = 0 \quad (18)$$

$$\sum_{j=1}^{2} A_{2j} \hat{X}_2 = \frac{1}{\sqrt{2}} (1 + 1) \hat{X}_2 = \frac{2}{\sqrt{2}} \hat{X}_2 \quad (19)$$

The suppression of one of the tones is shown in Fig. 6 where we again achieve a power difference of 30 dB.

We then recovered the constellations of two RF signals at 15 GHz of central frequency modulated using 16QPSK and 8PSK modulation. The results are shown in Fig. 7 with the independent signals shown in a) and c) and the received constellation when signals are not separated is presented in b). As with the
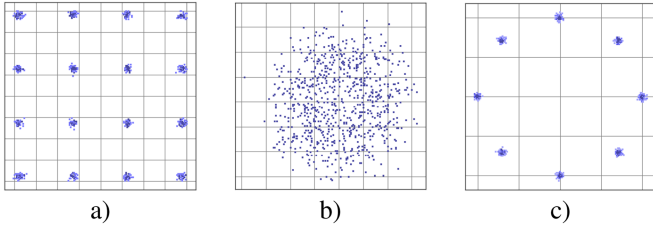
Fig. 7. Constellation evolution using $180°$ hybrid, only for the sum with an phase difference of 0 degrees, (a) and (c), do we recover the original constellations, for intermediate offsets, (b), we observe an interference between the two of them.
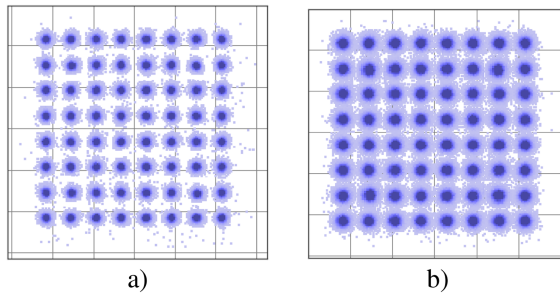
Fig. 8. Constellation for 5G signals at 50 MHz (a) and 100 MHz (b) for $180°$ hybrid. The result for the transmission of 5G signals is similar to those presented with the $90°$ hybrid, however we can observe a slight deterioration of the constellations. This is due to the different transmission characteristics of the hybrids used.

$90°$ hybrid, 5G signals at 50 MHz and 100 MHz are recovered. Results are presented in Fig. 8.

V. ANALOG PHOTONIC MIMO: PROPOSED ARCHITECTURE

One of the most computational expensive processes in massive-MIMO corresponds to the multiplication of large matrices. Standard matrix multiplication algorithms require $\mathcal{O}(n^3)$ arithmetic operations. For large-scale computation, as it is the case in massive-MIMO systems, there exist more efficient algorithms that reduce the complexity to $\mathcal{O}(n^{2.81})$ (Strassen [33]) or $\mathcal{O}(n^{2.373})$ (Le Gall [34]) [35]. In the following section, we introduce a novel analog system with a coherent photonic processor for the unscrambling of RF signals in the optical domain. The proposed architecture is shown in Fig. 9 and is based on a Silicon-On-Insulator (SOI) platform. SOI has become the predominant platform for optical links and future optical processors thanks to its compatibility with the available CMOS technology [36].

The proposed system consists of an up-conversion stage where the RF signal is converted into the optical domain. The resulting signal is filtered and only one of the SB is left. Then we have the optical matrix multiplier which can implement any complex-valued matrix $\boldsymbol{B} \in \mathbb{C}^{N \times M}$ via SVD decomposition, where N is the number of inputs and M is the number of outputs. The final stage corresponds to the direct photodetection of the optical signal and the amplification of the detected RF signals. In order to preserve the amplitude and the phase changes of the RF

signal, carrier reinsertion is necessary before the photodetection, see Section III.

In a previous work, Salmani, M. et al. [21] presented an optical processor for massive-MIMO systems that is based on B&W. This type of systems rely on the use of MRRs and wavelength division multiplexing (WDM). It presents some advantages over our presented architecture, specially in terms of footprint, but on the other hand, are inherently unable to implement complex matrix multiplications introducing extra pre- and post-processing steps. An extensive review of the capabilities of both architectures in terms of energy efficiency, optical losses and scalability as already been studied [37].

A. Up-Conversion and Filtering

The first step of the analog photonic architecture is to up-convert the incoming RF signal into the optical domain. To do so, a single wavelength light source is necessary. We proposed the use of a 1550 nm off-circuit laser to be compatible with current optical communication schemes. Emitted light is guided using single mode optical fiber (SMF) and fiber poralization controllers. External light sources present temperature stability and high light emission efficiency but are affected by the usually high coupling losses with the silicon microwave integrated circuit. Fiber-to-chip interface can be done via in-plane or out-of-plane couplers. In-plane couplers offer high coupling efficiencies, achieving theoretical losses of 0.6 dB with negligible polarization dependence but optical-quality facets need to be realized on integrated circuit. Meanwhile, vertical coupling offers easier lithographic fabrication [38]. As a future alternative, on-chip light sources promise to bring higher integration density and lower energy consumption but the technology is not mature enough [39].

Once the light is coupled into the photonic microwave integrated circuit, an splitter tree consisting of cascaded 3-dB MMI spatially multiplexes the optical signal into $N + 1$ independent paths, where N corresponds to the number of inputs in the optical matrix multiplier. An extra path will be needed for the reinsertion of the optical carrier before photodetection.

Next, the RF signals coming from the N antenna receivers are modulated into the optical domain using high-speed silicon modulators. High-performance Mach Zehnder Modulators (MZM) based on the plasma dispersion effect are commercially available from current silicon foundries, achieving bandwidths up to 40 GHz [40], [41]. Hybrid integration can open the path to higher modulation bandwidths on the order of 100 s GHz [42], [43]. At the end of this stage, the optical carrier and one of the SB are filtered. Microwave filters integrated in silicon photonics have been widely studied and experimentally demonstrated [44].

B. Optical Matrix Multiplier

The optical matrix multiplier consists of a mesh of optical interferometers. The basic computational unit (BCU) of the mesh is a 2×2 balanced Mach Zehnder Interferometer made up of two 3-dB MMI couplers, a phase actuator (θ) in one of the internal arms and another phase actuator (ϕ) in one of the external arms [45]. An example of this BCU is shown in Fig. 9
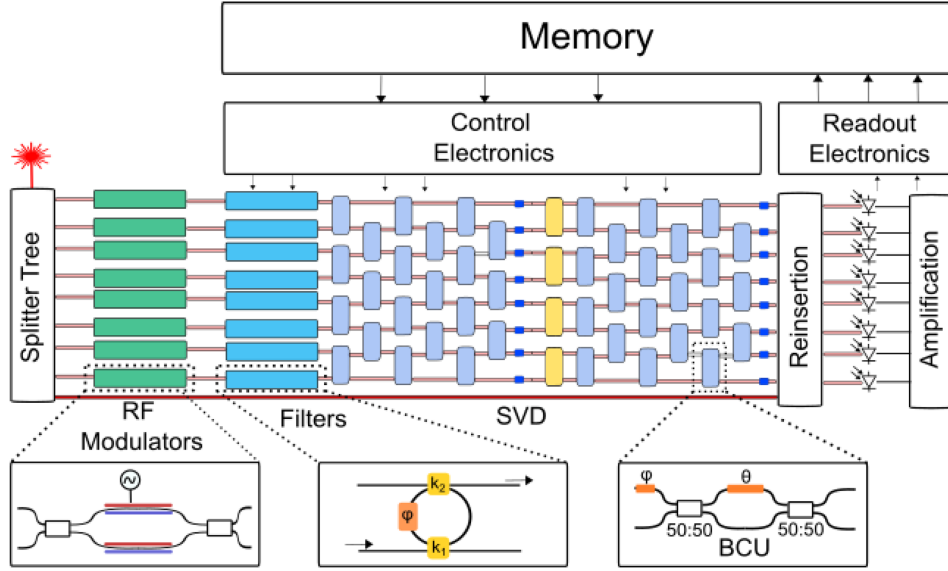
Fig. 9. General scheme of the proposed photonic MIMO processor. The input optical laser is spatially multiplexed using an splitter tree made up of 1x2 MMI. The optical signals are then modulated with the RF signals coming from the antenna receivers, and one of the side-bands is filtered along with the optical carrier. One of the optical signals (lower path) is not modulated and serves for the carrier re-injection. The filtered signals are unscrambled using the optical matrix multiplier. A general matrix is implemented using the SVD decomposition. At the output of the matrix multiplication the optical carrier is reinserted and the resulting signals are photodetected and amplified. The complete system is controlled by a set of electronic devices.

and can implement the following unitary transformation:

$$U(2) = \begin{pmatrix} e^{i\phi}sin(\frac{\theta}{2}) & e^{i\phi}cos(\frac{\theta}{2}) \\ cos(\frac{\theta}{2}) & sin(\frac{\theta}{2}) \end{pmatrix} \quad (20)$$

The individual BCUs can be combined to create higher dimensional interferometers. The triangular arrangement proposed by Reck, et.al [46] and the rectangular arrangement proposed by [47] are the most common approaches. These architectures allow the implementation of universal unitary $U(N)$ transformations over an N-dimensional Hilbert space as $|y\rangle = U|x\rangle$. In our proposed architecture, the unitary matrices are implemented using a rectangular mesh of interferometers which provide a more compact and loss balanced scheme than the triangular architecture. The phase shift values of each of the BCU that bring the desire $N \times N$ unitary transformation can be calculated using the decomposition algorithm [47]. After this process, the transformation U is divided in a product of the unitary transformations of each individual BCU as

$$U(N) = D \left(\prod_{(n,m)\epsilon S} T_{n,m}(\phi,\theta) \right) \quad (21)$$

where $T_{n,m}(\phi,\theta)$ is the transformation of a single BCU between modes n, m in an N-dimensional space and D is a diagonal matrix where the nonzero elements have unit modulus. The number of necessary BCUs is $\frac{N(N-1)}{2}$ in this arrangement. The total number of phase actuators scales as $\mathcal{O}(N^2)$, two per BCU plus a final row of N actuators that correspond to the diagonal matrix. Phase actuators can be design to harness the thermo-optic effect [48], a micro-electromechanical effect (MEMS) [49] or

the pockels effect, that aims to reduce the switching time under the microsecond scale [50].

Real channel matrices in massive-MIMO are, in general, not unitary and our analog photonic MIMO processor must implement any arbitrary complex valued matrix. It can be shown that any real or complex matrix $B^{N \times M}$ can be factorized using the SVD decomposition method as $\boldsymbol{B} = U\Sigma V$, where U and V are $N \times N$ and $M \times M$ unitary matrices respectively, and Σ is a non-squared $N \times M$ diagonal matrix. The combination of these method with the mesh of interferometers has been previously discussed in the literature [22]. The diagonal matrix can be straightforwardly implemented using single MZI as optical attenuators, see the orange column of BCU at Fig. 9. Although the SVD decomposition presents a computational complexity of the same order as the matrix multiplication it should be noted that the SVD step must be done only once for each coherence time of the channel. During this time a large number of multiplications are implemented and no advantage of the photonic processor over electronic systems is lost. Alternatively, the BCUs can also be tuned to implement the desire matrix without the SVD step using self-configuration techniques [27]. Along with the photonic mesh interferometer there is a non-interacting optical path in the lower part of the optical matrix processor. Here, the optical carrier is guided for its reinsertion before photodetection. Mathematically our $N \times M$ optical matrix becomes an $(N+1) \times (M+1)$ matrix where the extra row and column are full of zeros except on the element $(N+1, M+1)$ which is equal to 1. This expansion of the integrated photonic matrix was experimentally demonstrated for complex-valued operations by Zhang, H. et al. at [51] although their photodetection scheme differs from our proposal. The calibration of the system can be performed with external photodetectors as presented by [52].

TABLE I
PARAMETERS USED FOR THE ANALYSIS OF THE FIGURES-OF-MERIT OF THE SYSTEM

Data Rate	DR	10 GS/s
Laser wall-plug efficiency	η_{WPE}	10%
Input optical power	P_{in}	30 mW
Thermo-optic phase shifter π-shift power consumption	$P_{\pi-TO}$	20 mW [57]
Power consumption of Mach Zehnder Modulator	P_{MZM}	480 mW [58]
Energy consumption of photodetection and amplification	E_{PD-TIA}	2.3 pJ/b [59]
Memory interface power consumption	P_{mem}	5.77 mW [37]

C. Reinsertion and Photodetection

Once the signals have been multiplied and, in principle, unscrambled, the outputs of the matrix have to be photodetected and the corresponding RF signals detected. Our architecture will use high-speed envelope photodetectors. High-speed photodetectors compatible with the silicon photonics foundries technology have been reported and validated [40], [53], [54] As explained in Section III, when no balanced photodetection is used, the reinsertion of the optical carrier is necessary. For this reinsertion we propose to divide the optical carrier that is at the $M + 1$ output of the optical matrix into M paths using an optical splitter tree made up of 1×2 MMI couplers. Each of these paths is combined with each of the M remaining outputs of the matrix using 2×1 MMI couplers. The resulting signal is photodetected and the received RF signals preserves the changes suffered during the matrix multiplication in both amplitude and phase. After the photodetection, a high-speed CMOS transimpedance amplifier (TIA) [55] is located out of the microwave integrated circuit to enhance quality of the signal.

D. Electronics

The photonic analog processor works together with a set of electronic systems. On the one hand, it is necessary to have the proper control electronics to configure the weight parameters of the optical matrix multiplier and manage the working regimes of the filters, modulators and photodetectors. On the other hand we need a readout circuitry to process the RF output signals. The correct design of a Printed Circuit Board (PCB) perfectly adapted for high frequencies and without interferences is essential. Achieving precise timing synchronization between ADCs and DACs in high-speed data processing systems is a critical challenge. This requires accurate clock distribution, delay compensation techniques, calibration procedures, and careful design of the system layout and signal routing to minimize signal reflections and crosstalk [58]. Finally, an electronic processor takes control of said circuits and is responsible of loading and saving the information in the external random access memory.

E. System Analysis

In this section we analyze some figures-of-merit of the analog photonic processor. We focus our study in the inference stage where the RF signals are unmixed using matrix multiplications. We consider square $N \times N$ matrices. Channel estimation is still realized by electronic processors. Future work will be needed to compare the capabilities of photonic processors during the

TABLE II
COMPUTATIONAL SPEED FOR DIFFERENT MATRIX SIZES

N	8	16	32	64	128
TMAC/s	2.56	10.24	40.96	163.84	655.36

estimation stage with current DSP systems. The parameters used for the estimates are presented in Table I.

1) Computational Speed: When matrix weights are kept constant for a wide range of input vectors the computational speed is limited by the data preparation and readout speed. For a complex-valued matrix multiplication, a conventional electronic processor will take $4N^2$ multiply-and-accumulate (MAC) operations. The total number of MAC/s achievable by the computational unit is:

$$MAC/s = 4N^2DR \qquad (22)$$

where DR stands for data rate. We assume a conservative DR of 10 GS/s that is easily obtained with the available technology. In Table II we show the computational speed for different matrix sizes.

To satisfy the previous claim, photonic integration technology should solve the resolution challenge associated with the signal-to-noise ratio of the system. In particular, under the conditions expressed in Table I, the insertion loss of the BCUs should be reduced below 0.1 dB for larger scale systems beyond 32x32 multiplications (See Section V-E3), in order to reach an effective number of bits of 4. Other options are the use of avalanche photodetectors or the augmentation of the power handling capabilities at PIC level followed by a higher optical power value.

2) Power Consumption and Efficiency: The electrical power consumption of the entire system can be divided into the contributions of the different subsystems, the data preparation (laser and modulation), mesh configuration (phase shifters), readout (photodetection and amplification), and communication with the memory.

$$P = P_{laser} + NP_{mod} + N^2P_{PS} + NP_{PD-TIA} + P_{mem} \qquad (23)$$

Using the parameters of Table I we calculate the power consumption and energy efficiency for different matrix sizes. The results are presented in Table III.

The photonic architecture can achieve energy efficiencies one order of magnitude higher than current GPU, that work in the order of 100 s GFLOPs per Watt [59].

3) Scalability: The size of the matrix that can be implemented in the analog processor is limited by the optical losses that degrade the signal when it goes through the modulators,

TABLE III
POWER CONSUMPTION AND ENERGY EFFICIENCY FOR DIFFERENT MATRIX
SIZES

N	8	16	32	64	128
Power (W)	5.6	13.47	36.88	114.42	392.37
E/MAC (pJ/MAC)	2.19	1.32	0.90	0.70	0.60
TMACs / W	0.46	0.76	1.11	1.43	1.67

heaters and splitters. The optical power at the PD can be described as

$$P_{PD} = P_{laser} - IL_{SplitterTree} - IL_{mod} - 2NIL_{MZI}$$
(24)

where IL represent the insertion losses of the devices. The $IL_{SplitterTree}$ are $10log(N) + log_2(N)EL$, where EL are the excess losses of the individual splitter. If we want a conservative 10 dB SNR at the photodetectors we need an optical power of -21.6 dBm [60]. Assuming splitter excess losses of 0.1 dB, modulator losses of 4 dB and MZI insertion losses of 0.4 dB and an input optical power of 15 dBm the maximum size of the matrix core is 23×23. The size of the core can be improved if optical amplifiers are placed in the diagonal matrix between the two unitaries. If the matrix to be multiplied has a higher dimension than the available at the optical core the matrix must be decomposed into lower dimension blocks and sequential algorithms must be applied. Note that the 10 dB SNR is directly associated to a resolution of less than 2 effective bits. To meet larger scale demands (transformations of 32 or 64 antennas) and resolutions of 10 bits the system would require a loss per BCU below 0.06 dB and 0.02 dB, respectively. Current commercial systems have already achieve a size of 64x64 with a computing capacity of 8 TOPS [61]. In addition, the system could be pumped with more optical power at the laser front, but power handling capabilities of silicon photonics is typically limited to a maximum of 17 dBm due to inherent system nonlinearities. A platform combining silicon nitride and silicon is ideal to cope with the high power, high-performance systems and large-scalability demands.

F. Simulation

In this part, we simulate the performance of the proposed architecture in a real MIMO problem using the theory developed in Section III. We generate random channel matrices and assume that they are known by both the transmitter and the receiver. The RF signals are modulated using a QPSK modulation at 25 GHz carrier frequency. The signals are optically modulated and filtered assuming ideal behaviour. We chose a single-wavelength optical source at 1550 nm.

The optical processor is simulated following the MZI-based architecture explained in Section V-B. We study the accuracy of the system in terms of Bit Error Rate (BER) as a function of the MZI manufacturing errors. We have compared the error in implementing a desired matrix in the optical processor when the MZIs have imperfections in the MMI coupling coefficients (K) and phase terms (ϕ and θ) using Monte Carlo analysis. The operation of each MZI from the matrix can be modeled with Gaussian random variables centered at their ideal values, having a standard deviation σ_K, σ_ϕ and σ_θ [62]. Following results from
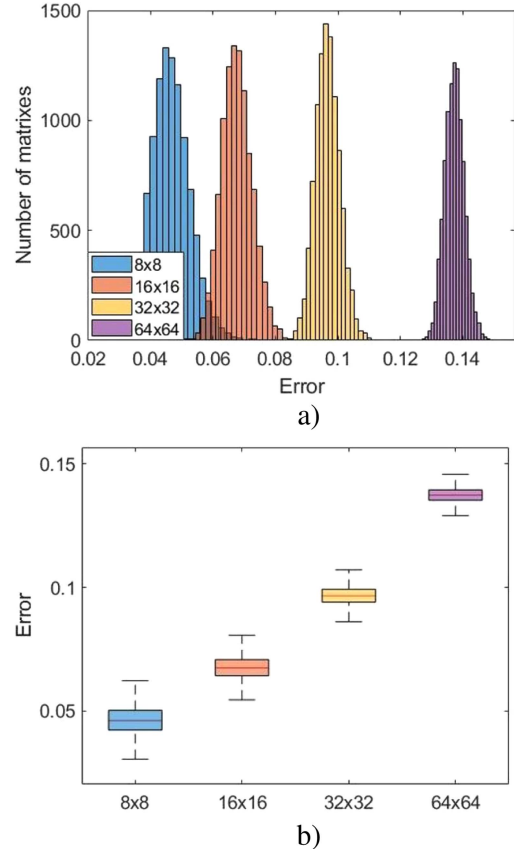
Fig. 10. Simulation of unitary matrices with manufacturing errors for different dimensions, (a) and (b) its statistical errors with respect to the desired matrix.

the literature, we found reasonable assuming a deviation of 1% both for coupling coefficients and phase terms. The impact of these deviations on the generated matrices for the generated matrices are shown in Fig. 10. For the case of an 8×8 matrix we study the impact on the recovered constellations for different values of SNR. Results are presented in Fig. 11.

The error is calculated as the squared norm of the difference between the desired matrix and the one obtained with the MZIs. The results of the error simulation are presented in Fig. 12 and show that scaling the dimensions of the matrices increases the difference with respect to the desired matrix, reaching a difference of 14% for 64×64 unitary matrices. Regarding the errors caused by the matrix engine, recent works have proposed innovative approaches to reduce the impact of fabrication errors [63] and adapt the engine to be aware of the intrinsic noise of high-speed systems [64].

Photonic core is formed by two unitary matrices due to the SVD. We have studied how this would affect to the system performance for different Signal to Noise Ratio of the RF signals. The larger the dimension of the matrix, the higher sensitivity to inter-channel interference, multipath propagation and noise and also the greater the effect of the accumulated errors in the two units that compose the photonic core.

The larger the dimension of the matrix, the greater the effect of the accumulated errors in the two units that compose the photonic core.
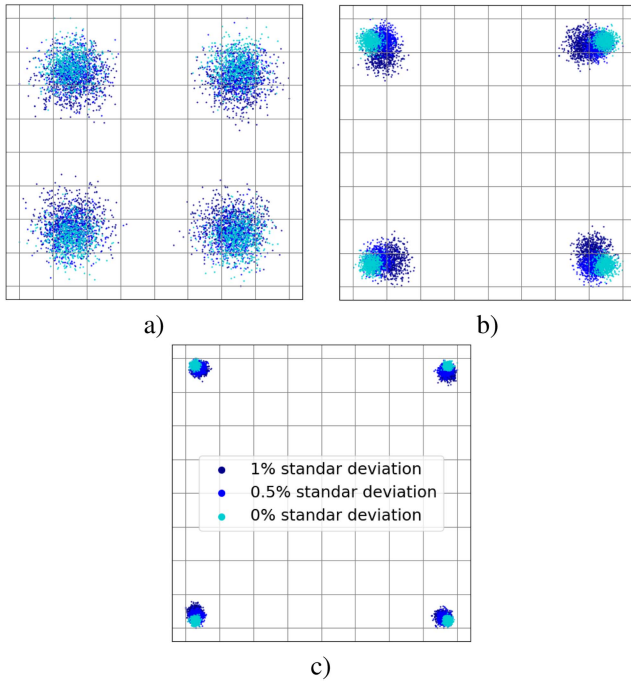
Fig. 11. Recovered constellations on an 8x8 dimension system for (a) 0 dB, (b) 10 dB and (c) 20 dB of SNR. As the noise value is reduced, it is easier to notice the contributions to the error in the constellations caused by the deviations in the parameters from the optical matrices.
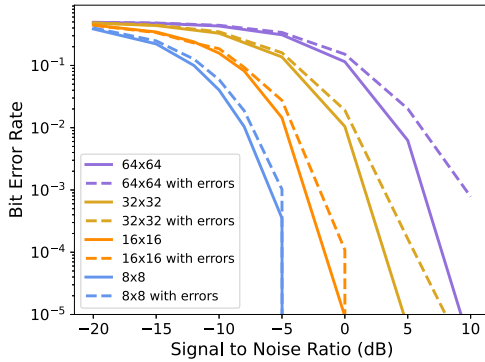
Fig. 12. Effect of errors for real channel matrices, with dimensions from 8x8 to 64x64 for different SNR.

VI. CONCLUSION

The increase of computational requirements in wireless communication systems has bring the need to explore alternatives ways of computation, faster and with less power consumption. In this paper, a theory to perform the unscrambling of RF signals by up-converting them into the optical domain has been developed, thus speeding up the processing of massive-MIMO signals and optimizing power consumption. We carry out an experimental proof of concept of this theory, where a dual-parallel Mach Zehnder Modulator is used for implementing 2×2 unitary transformations in the optical domain, recovering RF signals at 15 GHz with 20 MHz of bandwidth using 16QPSK and 8PSK modulation respectively and then with 5G signals with 50 and 100 MHz of bandwidth.

Finally, we introduce a novel photonic computing architecture based on a core of Mach Zehnder Interferometers in a feed-forward rectangular configuration that implements complex matrix multiplications in parallel. This architecture consists of an optical core, high-speed RF modulators, microwave photonic filters, high-speed photodetectors and the control electronics are introduced. To evaluate the capabilities of the photonic processor we performed theoretical simulations and studied the figures-of-merit, seeing that the processing of RF signals in the optical domain takes advantage of the high-bandwidth, parallelism and low latencies of the photonic systems.

REFERENCES

[1] I. Tomkos, D. Klonidis, E. Pikasis, and S. Theodoridis, "Toward the 6G network era: Opportunities and challenges," *IT Professional*, vol. 22, no. 1, pp. 34–38, 2020.

[2] Y. Qian, "Beyond 5G wireless communication technologies," *IEEE Wireless Commun.*, vol. 29, no. 1, pp. 2–3, Feb. 2022.

[3] T. R. Raddo et al., "Transition technologies towards 6G networks," *EURASIP J. Wireless Commun. Netw.*, vol. 2021, no. 1, Apr. 2021, Art. no. 100, doi: 10.1186/s13638-021-01973-9.

[4] E. G. Larsson, O. Edfors, F. Tufvesson, and T. L. Marzetta, "Massive MIMO for next generation wireless systems," *IEEE Commun. Mag.*, vol. 52, no. 2, pp. 186–195, Feb. 2014.

[5] F. W. Vook, T. A. Thomas, and E. Visotsky, "Massive MIMO for mmWave systems," in *Proc. IEEE 48th Asilomar Conf. Signals, Syst. Comput.*, 2014, pp. 820–824.

[6] W. Saad, M. Bennis, and M. Chen, "A vision of 6G wireless systems: Applications, trends, technologies, and open research problems," *IEEE Netw.*, vol. 34, no. 3, pp. 134–142, May/Jun. 2020.

[7] N. Jones et al., "The information factories," *Nature*, vol. 561, no. 7722, pp. 163–166, 2018.

[8] N.-P. Diamantopoulos, B. Shariati, and I. Tomkos, "On the power consumption of MIMO processing and its impact on the performance of SDM networks," in *Proc. IEEE Opt. Fiber Commun. Conf. Exhib.*, 2017, pp. 1–3.

[9] D. A. B. Miller, "Attojoule optoelectronics for low-energy information processing and communications," *J. Lightw. Technol.*, vol. 35, no. 3, pp. 346–396, Feb. 2017.

[10] T. N. Theis and H.-S. P. Wong, "The end of Moore's law: A new beginning for information technology," *Comput. Sci. Eng.*, vol. 19, no. 2, pp. 41–50, 2017.

[11] D. Marpaung, J. Yao, and J. Capmany, "Integrated microwave photonics," *Nature Photon.*, vol. 13, no. 2, pp. 80–90, Feb. 2019, doi: 10.1038/s41566-018-0310-5.

[12] D. Pérez et al., "Multipurpose silicon photonics signal processor core," *Nature Commun.*, vol. 8, no. 1, Sep. 2017, Art. no. 636, doi: 10.1038/s41467-017-00714-1.

[13] L. Zhuang, C. G. H. Roeloffzen, M. Hoekman, K.-J. Boller, and A. J. Lowery, "Programmable photonic signal processor chip for radiofrequency applications," *Optica*, vol. 2, no. 10, pp. 854–859, Oct. 2015. [Online]. Available: http://opg.optica.org/optica/abstract.cfm?URI=optica-2-10-854

[14] J. Chang and P. R. Prucnal, "A novel analog photonic method for broadband multipath interference cancellation," *IEEE Microw. Wireless Compon. Lett.*, vol. 23, no. 7, pp. 377–379, Jul. 2013.

[15] T. Shi et al., "Sub-Nyquist optical pulse sampling for photonic blind source separation," *Opt. Exp.*, vol. 30, no. 11, pp. 19300–19310, May 2022. [Online]. Available: http://opg.optica.org/oe/abstract.cfm?URI=oe-30-11-19300

[16] M. P. Chang, C.-L. Lee, B. Wu, and P. R. Prucnal, "Adaptive optical self-interference cancellation using a semiconductor optical amplifier," *IEEE Photon. Technol. Lett.*, vol. 27, no. 9, pp. 1018–1021, May 2015.

[17] M. P. Chang, E. C. Blow, J. J. Sun, M. Z. Lu, and P. R. Prucnal, "Integrated microwave photonic circuit for self-interference cancellation,"

IEEE Trans. Microw. Theory Techn., vol. 65, no. 11, pp. 4493–4501, Nov. 2017.

[18] W. Zhou, P. Xiang, Z. Niu, M. Wang, and S. Pan, "Wideband optical multipath interference cancellation based on a dispersive element," *IEEE Photon. Technol. Lett.*, vol. 28, no. 8, pp. 849–851, Apr. 2016.

[19] C. Huang et al., "High-capacity space-division multiplexing communications with silicon photonic blind source separation," *J. Lightw. Technol.*, vol. 40, no. 6, pp. 1617–1632, Mar. 2022.

[20] V. J. Urick, J. F. Diehl, C. E. Sunderman, J. D. McKinney, and K. J. Williams, "An optical technique for radio frequency interference mitigation," *IEEE Photon. Technol. Lett.*, vol. 27, no. 12, pp. 1333–1336, Jun. 2015.

[21] M. Salmani, A. Eshaghi, E. Luan, and S. Saha, "Photonic computing to accelerate data processing in wireless communications," *Opt. Exp.*, vol. 29, no. 14, pp. 22299–22314, Jul. 2021. [Online]. Available: http://opg.optica.org/oe/abstract.cfm?URI=oe-29-14-22299

[22] D. A. B. Miller, "Self-configuring universal linear optical component [invited]," *Photon. Res.*, vol. 1, no. 1, pp. 1–15, Jun. 2013. [Online]. Available: http://opg.optica.org/prj/abstract.cfm?URI=prj-1-1-1

[23] Y. Shen et al., "Deep learning with coherent nanophotonic circuits," *Nature Photon.*, vol. 11, no. 7, pp. 441–446, Jul. 2017, doi: 10.1038/nphoton.2017.93.

[24] N. C. Harris et al., "Quantum transport simulations in a programmable nanophotonic processor," *Nature Photon.*, vol. 11, no. 7, pp. 447–452, Jul. 2017, doi: 10.1038/nphoton.2017.95.

[25] M. Prabhu et al., "Accelerating recurrent ising machines in photonic integrated circuits," *Optica*, vol. 7, no. 5, pp. 551–558, May 2020. [Online]. Available: http://opg.optica.org/optica/abstract.cfm?URI=optica-7-5-551

[26] A. Annoni et al., "Unscrambling light-automatically undoing strong mixing between modes," *Light: Sci. Appl.*, vol. 6, no. 12, Dec. 2017, Art. no. e17110, doi: 10.1038/lsa.2017.110.

[27] K. Choutagunta, I. Roberts, D. A. B. Miller, and J. M. Kahn, "Adapting Mach-Zehnder mesh equalizers in direct-detection mode-division-multiplexed links," *J. Lightw. Technol.*, vol. 38, no. 4, pp. 723–735, Feb. 2020.

[28] H. Zhou et al., "Self-configuring and reconfigurable silicon photonic signal processor," *ACS Photon.*, vol. 7, no. 3, pp. 792–799, Mar. 2020, doi: 10.1021/acsphotonics.9b01673.

[29] D. Tse and P. Viswanath, *Fundamentals of Wireless Communication*. Cambridge, U.K.: Cambridge Univ. Press, 2005.

[30] F. Rusek et al., "Scaling up MIMO: Opportunities and challenges with very large arrays," *IEEE Signal Process. Mag.*, vol. 30, no. 1, pp. 40–60, Jan. 2013.

[31] P. Morton, J. Khurgin, and M. Morton, "All-optical linearized Mach-Zehnder modulator," *Opt. Exp.*, vol. 29, Nov. 2021, Art. no. 37302.

[32] C. Tsokos et al., "Analysis of a multibeam optical beamforming network based on Blass Matrix architecture," *J. Lightw. Technol.*, vol. 36, no. 16, pp. 3354–3372, Aug. 2018.

[33] V. Strassen, "Gaussian elimination is not optimal," *Numerische Mathematik*, vol. 13, no. 4, pp. 354–356, Aug. 1969, doi: 10.1007/BF02165411.

[34] F. L. Gall, "Powers of tensors and fast matrix multiplication," in *Proc. 39th Int. Symp. Symbolic Algebr. Comput.*, 2014, pp. 296–303, doi: 10.1145/2608628.2608664.

[35] Y. Li, S.-L. Hu, J. Wang, and Z.-H. Huang, "An introduction to the computational complexity of matrix multiplication," *J. Oper. Res. Soc. China*, vol. 8, no. 1, pp. 29–43, Mar. 2020, doi: 10.1007/s40305-019-00280-x.

[36] R. Baets et al., "Silicon-on-insulator based Nano-photonics: Why, how, what for?," in *Proc. IEEE Int. Conf. Group IV Photon.*, 2005, pp. 168–170.

[37] M. Al-Qadasi, L. Chrostowski, B. J. Shastri, and S. Shekhar, "Scaling up silicon photonic-based accelerators: Challenges and opportunities," APL Photonics 7, 020902, 2021. doi: 10.1063/5.0070992.

[38] R. Marchetti, C. Lacava, L. Carroll, K. Gradkowski, and P. Minzioni, "Coupling strategies for silicon photonics integrated chips [invited]," *Photon. Res.*, vol. 7, no. 2, pp. 201–239, Feb. 2019. [Online]. Available: http://opg.optica.org/prj/abstract.cfm?URI=prj-7-2-201

[39] Z. Zhou, B. Yin, and J. Michel, "On-chip light sources for silicon photonics," *Light: Sci. Appl.*, vol. 4, no. 11, Nov. 2015, Art. no. e358, doi: 10.1038/lsa.2015.131.

[40] S. Y. Siew et al., "Review of silicon photonics technology and platform development," *J. Lightw. Technol.*, vol. 39, no. 13, pp. 4374–4389, Jul. 2021.

[41] K. Giewont et al., "300-mm monolithic silicon photonics foundry technology," *IEEE J. Sel. Topics Quantum Electron.*, vol. 25, no. 5, pp. 1–11, Sep./Oct. 2019.

[42] L. Alloatti et al., "100 GHz silicon organic hybrid modulator," *Light: Sci. Appl.*, vol. 3, no. 5, May 2014, Art. no. e173, doi: 10.1038/lsa.2014.54.

[43] A. J. Mercante et al., "110 GHz CMOS compatible thin film Linbo3 modulator on silicon," *Opt. Exp.*, vol. 24, no. 14, pp. 15590–15595, Jul. 2016. [Online]. Available: http://opg.optica.org/oe/abstract.cfm?URI=oe-24-14-15590

[44] Y. Liu, A. Choudhary, D. Marpaung, and B. J. Eggleton, "Integrated microwave photonic filters," *Adv. Opt. Photon.*, vol. 12, no. 2, pp. 485–555, Jun. 2020. [Online]. Available: http://opg.optica.org/aop/abstract.cfm?URI=aop-12-2-485

[45] S. Pai, B. Bartlett, O. Solgaard, and D. A. B. Miller, "Matrix optimization on universal unitary photonic devices," *Phys. Rev. Appl.*, vol. 11, Jun. 2019, Art. no. 064044. [Online]. Available: https://link.aps.org/doi/10.1103/PhysRevApplied.11.064044

[46] M. Reck, A. Zeilinger, H. J. Bernstein, and P. Bertani, "Experimental realization of any discrete unitary operator," *Phys. Rev. Lett.*, vol. 73, pp. 58–61, Jul. 1994. [Online]. Available: https://link.aps.org/doi/10.1103/PhysRevLett.73.58

[47] W. R. Clements, P. C. Humphreys, B. J. Metcalf, W. S. Kolthammer, and I. A. Walmsley, "Optimal design for universal multiport interferometers," *Optica*, vol. 3, no. 12, pp. 1460–1465, Dec. 2016. [Online]. Available: http://opg.optica.org/optica/abstract.cfm?URI=optica-3-12-1460

[48] S. Liu et al., "Thermo-optic phase shifters based on silicon-on-insulator platform: State-of-the-art and a review," *Front. Optoelectron.*, vol. 15, no. 1, Apr. 2022, Art. no. 9, doi: 10.1007/s12200-022-00012-9.

[49] H. Sattari et al., "Silicon photonic MEMS phase-shifter," *Opt. Exp.*, vol. 27, no. 13, pp. 18959–18969, Jun. 2019. [Online]. Available: http://opg.optica.org/oe/abstract.cfm?URI=oe-27-13-18959

[50] L. Czornomaz and S. Abel, "BTO-enhanced silicon photonics–A scalable PIC platform with ultra-efficient electro-optical modulation," in *Proc. Opt. Fiber Commun. Conf. Exhib.*, 2022, pp. 1–3.

[51] H. Zhang et al., "An optical neural chip for implementing complex-valued neural network," *Nature Commun.*, vol. 12, no. 1, Jan. 2021, Art. no. 457, doi: 10.1038/s41467-020-20719-7.

[52] C. Alexiev, J. C. C. Mak, W. D. Sacher, and J. K. S. Poon, "Calibrating rectangular interferometer meshes with external photodetectors," *OSA Continuum*, vol. 4, no. 11, pp. 2892–2904, Nov. 2021. [Online]. Available: https://opg.optica.org/osac/abstract.cfm?URI=osac-4-11-2892

[53] S. Lischke et al., "Ultra-fast germanium photodiode with 3-dB bandwidth of 265 GHz," *Nature Photon.*, vol. 15, no. 12, pp. 925–931, Dec. 2021, doi: 10.1038/s41566-021-00893-w.

[54] D. Benedikovic et al., "Silicon-Germanium avalanche receivers with fj/bit energy consumption," *IEEE J. Sel. Topics Quantum Electron.*, vol. 28, no. 2, Mar./Apr. 2022, Art. no. 3802508.

[55] K. R. Lakshmikumar, A. Kurylak, M. Nagaraju, R. Booth, and J. Pampanin, "A process and temperature insensitive CMOS linear TIA for 100 Gbps/λ PAM-4 optical links," in *Proc. IEEE Custom Integr. Circuits Conf.*, 2018, pp. 1–4.

[56] N. Hosseinzadeh, K. Fang, L. Valenzuela, C. Schow, and J. F. Buckwalter, "A 50-Gb/s optical transmitter based on co-design of a 45-nm CMOS soi distributed driver and 90-nm silicon photonic Mach-Zehnder modulator," in *Proc. IEEE/MTT-S Int. Microw. Symp.*, 2020, pp. 205–208.

[57] L. A. Valenzuela, A. Maharry, H. Andrade, C. L. Schow, and J. F. Buckwalter, "Energy optimization for optical receivers based on a Cherry-Hooper emitter follower transimpedance amplifier front-end in 130-nm SiGe HBT technology," *J. Lightw. Technol.*, vol. 39, no. 23, pp. 7393–7405, Dec. 2021.

[58] C. Pearson, "High-speed, analog-to-digital converter basics," Texas Instrum., Dallas, TX, USA, Appl. Rep. SLAA510, 2011.

[59] Y. Sun, N. B. Agostini, S. Dong, and D. Kaeli, "Summarizing CPU and GPU design trends with product data," 2019. [Online]. Available: https://arxiv.org/abs/1911.11313

[60] J. R. Rausell Campo and D. Pérez-López, "Reconfigurable activation functions in integrated optical neural networks," *IEEE J. Sel. Topics Quantum Electron.*, vol. 28, no. 4, Jul./Aug. 2022, Art. no. 8300513.

[61] H. Zhou et al., "Photonic matrix multiplication lights up photonic accelerator and beyond," *Light: Sci. Appl.*, vol. 11, no. 1, Feb. 2022, Art. no. 30, doi: 10.1038/s41377-022-00717-8.

[62] D. Pérez and J. Capmany, "Scalable analysis for arbitrary photonic integrated waveguide meshes," *Optica*, vol. 6, no. 1, pp. 19–27, 2019. [Online]. Available: http://www.osapublishing.org/optica/abstract.cfm?URI=optica-6-1-19

[63] S. Bandyopadhyay, R. Hamerly, and D. Englund, "Hardware error correction for programmable photonics," *Optica*, vol. 8, no. 10, pp. 1247–1255, Oct. 2021. [Online]. Available: https://opg.optica.org/optica/abstract.cfm?URI=optica-8-10-1247

[64] G. Mourgias-Alexandris et al., "Noise-resilient and high-speed deep learning with coherent silicon photonics," *Nature Commun.*, vol. 13, no. 1, Sep. 2022, Art. no. 5572, doi: 10.1038/s41467-022-33259-z.

Pablo Martínez-Carrasco Romero received the B.S. degrees in physics from the University of Valencia, Valencia, Spain, in 2020, and the M.S degree in telecommunication engineering from the Polytechnic University of Valencia, Valencia, Spain, in 2021. He is currently working toward the Ph.D. degree with Photonics Research Labs. In 2021, he joined the Photonics Research Labs. His research interests include photonic integrated circuits and its applications to signal processing and computing, including optical communication systems, and photonic beamforming architectures for wireless communications.

José Roberto Rausell-Campo received the B.S. and M.S. degrees in physics from the University of Valencia, Valencia, Spain, in 2018 and 2019, respectively. He is currently working toward the Ph.D. degree in telecommunications with the Polytechnic University of Valencia, Valencia, Spain. His research interests include nonlinear optics, optical information processing, and machine learning.

Diego Pérez-Galacho received the M.Sc. degree in telecommunication engineering from Málaga University, Málaga, Spain, in 2011. From 2011 to September 2013, he was with the design of coherent receivers in III-V Technology for the European Project MIRTHE with the Photonics and RF Research Laboratory, Málaga University. In September 2013, he joined the Silicon Photonics Research Group, Paris-Sud University, where he worked on the development of silicon transceivers for the European Projects PLAT4M and COSMICC. In October 2016, he defended my Ph.D. entitled High speed optical modulation, advanced modulation formats and mode division multiplexing in Silicon Photonics with Paris-Sud University, Orsay, France. Since October 2017, he has been with the Photonics Research Labs, Polytechnic University of Valencia, Valencia, Spain. His research interests include devices based on periodic structures and analog and digital optical communication systems, including polarization diversity and space division multiplexing, optical information processing, and integrated photonics.

Xu Li received the B.S. and Ph.D. degrees in electrical and electronics engineering from the University of Science and Technology of China, Hefei, China, in 2010 and 2015, respectively. From 2013 to 2014, he was a Visiting Ph.D. Student with the Department of Electrical Engineering and Computer Science, Northwestern University, Evanston, IL, USA. His research interests include various architectures of radio access network in 5G, especially the end to end network slicing. He has a rich wireless research experience, including ultra-wide band (UWB) chips, interference alignment, relay networks, stochastic geometry, and public safety wireless broadband networks. His current research topics include microwave wireless communication, radio over fiber communication, and optical wireless communication.

Ting Qing received the B.S., M.S., and Ph.D. degrees in electronic and information engineering from the Nanjing University of Aeronautics and Astronautics, Nanjing, China, in 2014, 2017, and 2021, respectively. Her research focuses on microwave photonics, especially the optical vector analysis. Her current research interests include radio over fiber communication, microwave photonics measurement, and photonic integrated chip.

Tiangxiang Wang is currently a Senior Technologist with the Wireless Technology Lab of Huawei Co. LTD. His research interests include optoelectronic integration for next generation mobile communication system and field system verification

Daniel Pérez-López (Member, IEEE) (M.Sc., Ph.D.), has spent his academic life on the creation, development of a programmable photonics, such as giving to large-scale photonic integrated circuits flexibility through run-time software programming. His career started with his Ph.D. and a two-year postdoc research with the Polytechnic University of Valencia's Photonics Research Labs, where he investigated novel photonic integrated circuit designs and architectures that can be reconfigured to perform multipurpose functionalities. These works led to the 2017 Graduate Student Fellowship by the IEEE Photonics Society and 2018 Extraordinary PhD Thesis Award from UPVLC. During 2019–2020, he was with Xanadu Quantum Computing, Canada, and founded iPronics Programmable Photonics S.L, Spain. Between 2019 and 2021, he was the recipient of the prestigious Juan de la Cierva Fellowship grants that allowed him to initiate his research on high-dense large-scale programmable photonic integrated circuits and its applications to signal processing and computing.